Advances in Aerodynamics

RESEARCH Open Access

High-speed rarefied gas flow over a cavity at different angles of attack

Oleg Sazhin[1*]

*Correspondence:
oleg.sazhin@urfu.ru

[1] Ural Federal University, Ekaterinburg 620000, Russia

Abstract

A numerical analysis of high-speed rarefied gas flow over a cavity has been performed using the direct simulation Monte Carlo (DSMC) method. The simulation was carried out over a wide range of gas rarefaction, from free-molecular flow to nearly continuum flow, for various values of the angle of attack, the free-stream Mach number, and the geometric size of the cavity. Flow fields, streamlines, vertical 1D distributions of macroscopic quantities, and the dimensionless particle flux density to the cavity floor were calculated with high accuracy. It was found that the flow pattern in the simulated system strongly depends on all flow parameters. At a certain distance from the cavity, the gas flow passes through a detached shock, where the flow regime changes from supersonic to subsonic. In close proximity to the cavity inlet, a complex flow structure can form, such as a flow separation zone, including a recirculation zone and a reverse flow zone. Inside the cavity, a circulating motion of the gas is formed, the pattern of which is significantly influenced by the geometric size of the cavity.

Keywords: Cavity flow, Rarefied gas, Mach number, Knudsen number, Direct simulation Monte Carlo method

1 Introduction

The problem of high-speed rarefied gas flow around an object is of significant importance in modern science and engineering. This issue has garnered substantial attention due to its direct impact on various technological advancements. Over recent decades, the study of high-speed rarefied gas dynamics has become increasingly relevant in the context of space exploration, as well as supersonic and hypersonic aircraft design. Additionally, this area of research plays a critical role in the development of vacuum technologies and micro- and nanofluidic devices [1–5].

Under high-speed and rarefied atmospheric conditions, aerodynamic phenomena become particularly complex. High-speed flights in such environments pose significant challenges for engineers and researchers, as understanding and managing aerodynamic effects is critical for ensuring stability and safety. Consequently, this area represents one of the primary challenges in modern aerodynamics, aerospace engineering, and related fields. This multifaceted problem demands a deep comprehension of the physical phenomena involved in high-speed gas dynamics within low-pressure environments.

Springer

A key aspect of this field is understanding the interactions between objects and rarefied gas at high speeds. These interactions are directly relevant to the design and functionality of spacecraft, reusable missiles, hypersonic aircraft, and similar systems. Among the most practically significant research directions, the following can be highlighted:

Firstly, the development of high-speed transportation systems capable of operating in rarefied atmospheres at high angles of attack represents a promising direction for aviation and transportation infrastructure. Precise control of an object's aerodynamic properties in rarefied gas flows is essential for maintaining stability and preventing adverse effects during high-speed maneuvers.

Secondly, satellites, spacecraft, and space shuttles encounter rarefied gas when entering planetary atmospheres or returning to Earth's atmosphere, where they experience complex aerodynamic and thermal effects. Understanding and controlling these effects are critical not only for ensuring safe descent but also for optimizing the efficiency and success of such missions.

Thirdly, the military sector is deeply involved in studying high-speed gas flows, particularly in the context of hypersonic weapons and aircraft, as effective maneuvering and operation under such conditions are of strategic importance.

Thus, the study of high-speed rarefied gas flows around an object has broad applications, significantly impacting engineering, transportation, and space exploration, driving modern scientific research and technological advancements.

Among the various streamlined objects, surface cavities hold a special place, as they are of both practical and theoretical interest. The latter, in particular, arises from the fact that the flow field in a cavity can exhibit both external and internal flow characteristics, while the flow regime itself can vary from free-molecular to viscous and even hydrodynamic. The practical significance of cavity studies is further emphasized by their substantial impact on temperature distribution and heat exchange. This aspect is particularly critical for designing thermal protection screens and cooling systems in high-speed vehicles. Due to its considerable importance, this topic is being extensively studied through experimental and numerical methods.

The available literature contains numerous experimental investigations on high-speed rarefied gas flow over cavities. For the sake of brevity, only the most frequently cited articles will be reviewed. Foundational works by Charwat et al. [6, 7] extensively examined separated regions such as blunt-base wakes and cavities under supersonic (Mach numbers 2 to 4) and subsonic flows. Their studies described conditions for existence, geometry, and pressure fields [6], as well as the internal flow and heat transfer across these regions [7].

Nestler et al. [8] studied heat flux distributions in rectangular cavities with the length-to-depth ratio from 0.2 to 30 at local Mach numbers of 6.3 and 8.5, and local Reynolds number of about 10^7. Semi-empirical correlations were suggested for relative heat flux ratios in terms of local dimensionless flow parameters.

In the Langley 0.3-m transonic cryogenic tunnel, the flow field observed at subsonic and transonic speeds in rectangular cavities with length-to-depth ratios of 4.4, 6.7, 12.67, and 20.0 for angles of attack (AOA) of 0° and 15° was studied using the complementary static

and fluctuating pressure data measured [9]. Flow field types were determined using static pressure measurements and acoustic tones identified from peaks in fluctuating pressure spectra and characteristic mode shapes in the cavity.

Compressible flows over cavities with a series of length-to-depth ratios have been investigated experimentally, with the objective to elucidate the physics of the transition of cavity-flow types as the length-to-depth ratio changes [10]. It was found that the freedom of backflow inside the cavity is crucial in smoothing out the adverse pressure gradient, and the effect of the upstream separation wake on the downstream compression wake is non-negligible.

A combined experimental/computational study of the cavity flow with length-to-depth ratios from 1 to 8 at low Reynolds and Mach numbers of 9 has been carried out [11]. According to this experimental study, for the shorter cavities, the good agreement between experiment and laminar CFD on the front and back faces of the cavity, as well as on the fore-body and after-body, is strong evidence for laminar flow. For the longer cavities, the early stages of the laminar-turbulent transition are observed.

In the Langley 31-inch Mach 10 tunnel, the effect of a pressure gradient on the local heating disturbance of rectangular cavities under hypersonic free-stream conditions has been assessed using the two-color phosphor thermography method [12]. It was discovered that for the short cavity geometries, the pressure gradient had minimal effect, if any, on the average heating augmentation of the cavity floor. For the long cavity geometries, the pressure gradient increased the average heating augmentation factor by 50% relative to the zero gradient conditions.

The effect of an isolated rectangular cavity on hypersonic boundary layer transition onset on the windward surface of the Shuttle Orbiter has been experimentally characterized [13]. It was found that an increase in the cavity length-to-depth ratio and Reynolds number produced an augmentation in cavity floor heating, indicative of the shear layer entering the cavity and impinging on the cavity floor.

Using the particle image velocimetry (PIV) technique, experiments have been carried out in order to investigate the flow structure past rectangular, triangular and semicircular cavities with a length-to-depth ratio of 2:1 in Reynolds numbers of 1230, 1460 and 1700 [14]. According to experiments, the maximum turbulence intensities occur at the cavity lid in the centerline section, and rectangular and triangular cavities have larger turbulence intensities compared to a semicircular cavity. In addition to cavity shapes, Reynolds number changes have some degree of influence on the structure of flow and turbulence quantities.

A novel technique of convective heat flux reduction on the nose surface of a spherically blunted cone by employing a forward-facing cavity combined with heat energy deposition inside the cavity has been presented [15]. The heat deposition is achieved by the exothermic reaction of a chromium film coated on the cavity surface. It was found that the overall surface mean heat flux reduction increased from 13% to 49% compared to the blunt body geometry and enhanced from 15% to 35% with reference to the cavity without heat deposition.

Using the cavity pressure measurements and the schlieren imaging, supersonic flow around an axisymmetric annular cavity on the cylindrical body with a nose cone has been examined at different angles of attack [16]. According to the study, the

characteristics of flow around the cavity (such as the configuration of a system of shock waves, pressure distribution, etc.) can depend not only on the particular values of the parameters (angle of attack, cavity length, Mach number, etc.), but also on the history of reaching these values. The range of boundary-value parameters, at which such a non-unique behavior of flows is possible, is called as the parametric hysteresis region by the authors.

Many approaches and methods exist for the numerical simulation of rarefied gas flows, and a comprehensive overview is provided in [5, 17]. At this point, we examine only the most recent works that use the direct simulation Monte Carlo (DSMC) method [18] and do not consider numerical studies based on the traditional approach, which treats gas flow as a continuum with macroscopic quantities that change continuously in space and time, and is based on the Navier–Stokes equations (NSEs). The correct application of NSEs is restricted to a specific range of rarefied gas flow: for Knudsen numbers (Kn) less than 10^{-3}, NSEs are applicable under the non-slip boundary conditions; for Knudsen numbers between 10^{-3} and 10^{-1}, the equations remain valid but with slip boundary conditions [19]. To address the problem of gas flow across a wide range of Knudsen numbers (rarefaction), methods from kinetic gas theory should be applied. The central equation in this theory is the Boltzmann equation (BE), an integro-differential equation for the distribution function. The DSMC method is a stochastic approach to solving the full BE and is an effective method for solving gas dynamics problems across all flow regimes, from hydrodynamic to free molecular flow.

Palharini et al. have studied rarefied hypersonic flows over two- and three-dimensional cavities at an altitude of 70 and 80 km in the Earth's atmosphere and at a free-stream Mach number of 25 [20–22]. Effects of the length-to-depth ratio on the number flux, pressure, skin friction, and heat transfer coefficients in the transition flow regime have been investigated. It was found that the application of a 2D cavity solution would significantly overestimate aerothermodynamic loads, which were several times larger than those observed in a 3D study [20]. The flow field structure characterization around and inside the cavities in the presence of chemical reactions has been performed [21]. The results showed that the peak values of the pressure coefficient and heat transfer coefficient were approximately 4.9 and 2.1 times higher than those for a smooth surface (i.e., a flat plate without a cavity) [22].

Guo et al. [23–26] studied the flow over various cavities by hypersonic rarefied flows at different altitudes. In particular, the flow characteristics of hypersonic rarefied flow over a cavity with different geometric parameters such as the length-to-depth ratio, the rearwall-to-frontwall height ratio, and frontwall/rearwall inclination have been examined [23]. Simulation has been made for the free stream at a Mach number of 8 and an altitude of 60 km. The effect of cavity geometric parameters on the shear layer and recirculation region has been presented. Particularly, it was found that the frontwall/rearwall inclination is probably a simple but effective way to control the recirculation region(s) to disappear or reappear.

By considering the cases such as the altitude of 20–60 km, the Mach number of 6–20, and the sweepback angle of 30°–90°, flow characteristics of a cavity with sweepback angle in near space were specified [24]. As a result, it was established that with the increase of altitude, both the primary and secondary recirculation regions contract so greatly that

they eventually separate. When increasing the Mach number, the velocity, pressure, and temperature within the cavity increase uniformly. As the sweepback angle increases, the maximum pressure nearby the trailing edge of the cavity decreases rapidly, whereas the influence of sweepback angle on velocity distribution and maximum temperature within the cavity is slight.

Simulation was made to reveal flow structures inside the cavity and aerodynamic surface quantities, including the pressure on and heat flux to the surfaces of three-dimensional cylindrical cavities [25]. The simulation cases are obtained by varying the cavity diameter-to-depth ratio from 10 to 2, the altitude from 50 to 90 km, and the free-stream Mach number from 13.4 to 33.5. Particularly, it was found that with the increase of cavity depth, the weaker pressure on and heat flux to the cavity floor appear, whereas the maximum pressure on and peak heat flux to the downstream curved sidewall seem to be unchanged. The flow and aerodynamic characteristics for the altitudes of 50, 60, and 70 km are similar but those for the altitude of 90 km exhibit a distinctly different behavior due to the severe rarefaction effect there. As the free-stream Mach number increases from 13.4 to 33.5, the maximum heat flux coefficient on the downstream curved sidewall only increases with a rate of about 7.7%, while the maximum wall pressure coefficient decreases with a rate of about 18.3%.

Study of the influence of flow control block on aerodynamic properties of an open cavity in rarefied hypersonic flows has been performed [26]. The free-stream parameters of a typical atmospheric environment at the altitude of 50 km were applied, and the effect of placement position and shape of the control block on the cavity flow field was evaluated. It was found that the square control block demonstrates the strongest flow control when compared to the circular, triangular, and wedged control blocks.

Xiang and Fang [27] studied the heat flux and flow characteristics of a cavity with a length-to-depth ratio of 6 in the free stream at a Mach number of 8, with the angle of attack α ranging from 0° to 60°. The authors claim that when $\alpha < 50°$, there is an oblique shock wave that prevents the stream from entering the cavity, while when $\alpha > 50°$, there is a detached shock wave and the flow can enter the cavity.

Lekzian [28] performed the simulation of rarefied flow past a cavity with injection from the rear wall of the cavity for different length-to-depth ratios (ranging from 1.5 to 5.5) and Mach numbers (5 to 25). Results show that injection does not affect the cavity vortex location and has no significant effect on the wall pressure coefficient and the friction coefficient. However, due to injection, the dimensionless temperature decreases significantly, and the average number flux increases. Enhancing the injection velocity would decrease the heat transfer coefficient and promote cooling effects.

Jiang et al. [29] studied the rarefied hypersonic flow over a cavity at the free-stream flow conditions similar to those employed by Palharini and Santos [22]. The effects of cavity shape and size on the flow-field structures and aerodynamic surface quantities, including pressure coefficient, skin friction coefficient, and heat transfer coefficient, have been explored. The results reveal that the aerodynamic heat flux is dramatically influenced by the cavity shape and size, while the aerodynamic force is mildly affected. The pressure, skin friction, and heat transfer coefficients over the surface display complex trends as the cavity shape and size change.

Jin et al. [30–34] made significant progress in studying hypersonic rarefied cavity flows. In particular, study of the hypersonic rarefied flows over a flat plate with two- and three-dimensional (2D and 3D) cavities, focusing on the effect of the free-stream angle of attack and the 3D property on flow structure inside the cavity and aerodynamic surface quantities, has been carried out [30]. The authors claim that the assumption of two-dimensionality would overestimate heat transfer and pressure on the cavity surfaces. In the 3D cavity configuration, the two additional side surfaces play a role of a frictional wall and an energy sink, serving to not only block the entry of gas molecules coming from the main stream into the cavity, causing a reduction in the density inside the cavity, but also lighten the burden of heat loads of all the three cavity surfaces, resulting in a decrease in heat flux and pressure over them when compared with the 2D case. The length and width of the cavity used in the calculations were 3 mm and 12 mm, respectively. These dimensions are comparable to those reported in Ref. [20], and thus, similar effects of the side surfaces in the 3D case are expected to be observed.

Numerical calculation has been conducted to investigate a rarefied hypersonic flow past a 3D cavity with a length-to-depth ratio of 4 in the representative atmospheric environment at altitudes of 70, 75, 80 and 90 km [31]. The effects of Maxwellian accommodation coefficient and free-stream Knudsen number on flow field characteristics inside the cavity and aerodynamic surface quantities on the cavity surfaces, i.e., the pressure, shear stress, and heat flux, have been analyzed. The results emphasize the sensitivity of flow field characteristics and aerodynamic surface quantities to the accommodation coefficient and free-stream Knudsen number. It was also found that as the free-stream Knudsen number is augmented, the ability of the external stream to enter the cavity is lowered, causing the flow pattern inside the cavity to develop from a closed flow with two vortices generated into an open flow with only one vortex produced. From the other side, the two vortices inside the cavity move closer to each other and may merge into one when the gas-surface scattering changes from diffuse into specular reflection.

It is worth mentioning that specular reflection is almost never observed in practice. In our experiment [35, 36], we obtained a minimal value of the Maxwellian accommodation coefficient (0.71) on the atomically clean surfaces of silver and titanium for extremely pure helium gas (He). According to available published works (see review [37]), this is one of the lowest values obtained from experiments on internal rarefied gas flows, smaller than those reported in Refs. [38–40]. In particular, Cooper et al. [38] got a value of 0.52 when studying flow of argon, nitrogen, and oxygen through carbon nanotubes with a diameter of 200 nm. Keerthi et al. [39] got reflection close to specular reflection in the experiment of gas transport through ångström-scale channels with atomically flat walls. However, due to the nanoscale, quantum effects already manifest in these experiments [38, 39], and their nature in gas-surface scattering is not fully understood. In real situations for conventional gases (for example, air) on technical surfaces, gas-surface scattering is close to diffuse reflection; and for engineering calculations, a Maxwellian accommodation coefficient of 0.9 can be used [37].

The rarefied hypersonic flow past a group of 2D rectangular cavity configurations with rounded corners has been investigated [32]. Free-stream parameters were representative of the typical atmospheric environment at an altitude of 80 km (Knudsen number: 0.37; Mach number: 26.77), and the effects of rounding the separation/reattachment corner

on flow characteristics and aerodynamic surface quantities, i.e., the pressure and heat flux, were analyzed. The authors established that rounding the separation corner does not alter the streamline patterns too much, while rounding the reattachment corner brings about a remarkable effect on the streamline patterns. Eventually, they concluded that the approach of rounding the reattachment corner can achieve the most dramatic drop in the peak pressure and heat flux at the reattachment point.

Simulation for rarefied hypersonic flows past a flat plate with a 2D/3D rectangular cavity in the transition regime has been performed to obtain an illustrative understanding of the effects of the boundary layer thickness at the cavity entrance on flow field characteristics and quantitatively assess the sensitivity of aerodynamic quantities to the entrance boundary layer thickness [33]. It was found that the boundary layer thickness at the cavity entrance has strong effects on the flow past the 2D cavity, and the 3D effect plays an important role only for the cases of extremely thick boundary layers at the cavity entrance.

Rarefied hypersonic flows past various non-rectangular cavity configurations have been investigated to obtain insight into the flow characteristics, and surface pressure on and heat flux to these non-rectangular cavities [34]. Specifically, it was discovered that for the shallow-rear cavity, the surface pressure and heat flux at the right end of the cavity floor are 2 and 20 times higher than the values for the rectangular cavity, respectively. Reducing the free-stream Mach number from 25 to 10 does not bring about an obvious difference in flow patterns inside the cavity.

By analyzing the available literature, we can conclude that the problem of high-speed rarefied gas flow over a cavity is not only a fundamental issue but also holds greater practical significance. However, no published works have studied this problem across a wide range of Knudsen numbers (gas rarefaction). The goal of the current work is to provide a detailed study of high-speed rarefied gas flow over a cavity at different angles of attack in a wide range of gas rarefaction, covering flow regimes from free molecular to near-hydrodynamic.

Due to the strong non-equilibrium of the problem (high-speed flow), to achieve the set goal, it is appropriate to use the direct simulation Monte Carlo (DSMC) method [18], which, as mentioned above, is an effective tool for solving gas dynamics problems in all flow regimes—from free molecular to hydrodynamic. This method allows accounting for many factors, such as strong non-equilibrium, the complex geometrical configuration of the modeled system, and the use of various gas-surface scattering laws, surface structure models, and intermolecular potential models.

A reliable foundation for the successful completion of this study is our previous work, particularly our recent studies [41–45], where the DSMC method was used to obtain with high-accuracy dependencies of gas mass flow rate and flow field in channels of various shapes on a wide range of governing parameters, such as gas rarefaction and free-stream velocity, the reduced channel length (length-to-height ratio), pressure ratio (output pressure to input pressure of the channel), and parameters characterizing gas molecule scattering by the surface and intermolecular interactions in gas.

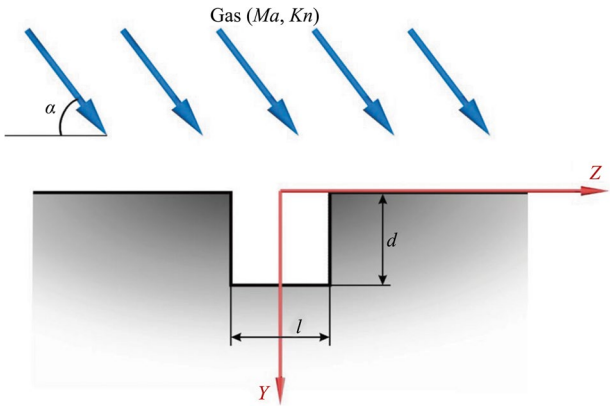

Fig. 1 Gas flow configuration over the cavity and coordinate system

2 Problem statement

Let us consider the steady state of rarefied gas attack on a flat surface at an angle α (AOA) with a free-stream velocity U. The free-stream velocity and rarefaction of the gas can be described by the Mach number Ma and Knudsen number Kn, respectively. The temperature and number density of the undisturbed gas (when $U=0$) are denoted as T_0 and n_0, respectively. The surface temperature in the entire simulated system is also equal to T_0. On the surface, there is a rectangular cavity with length l, depth d, and width w. Figure 1 shows the gas flow configuration over the cavity and the coordinate system. We will be interested in the gas flow field both inside the cavity and near it. We assume that the width of the cavity w is much greater than the other geometric dimensions l and d. In this case, the gas flow field can be assumed to be homogeneous along the X-axis, which makes it possible to reduce the problem to a two-dimensional physical domain while retaining a three-dimensional velocity space (2D3V).

In this work, we have developed our program code, which was previously used for high-precision simulation of high-speed rarefied gas flow through channels with a forward- or backward-facing step [45]. As before, we will use the DSMC method, based on the majorant frequency scheme [46], a three-level spatial grid, and special DSMC procedures, namely, cell subdivision into sub-cells and weighting planes. For modeling intermolecular interactions, we will apply the hard-sphere model, and the law of fully diffuse scattering will be used as the scattering law for gas molecules on the surface of a solid body.

Figure 2 shows the computational domain and spatial grid for modeling gas flow over a cavity. As can be seen from the figure, the computational domain has closed (solid line) and open (dashed line) boundaries. On the closed boundaries, the scattering law for gas molecules on the surface is applied. On the open boundaries, the so-called inlet and outlet boundary conditions are specified. In this work, we used explicit (typical) boundary conditions, according to which the inflow and outflow of particles into and from the simulated system occur far from the cavity. Specifically, new particles enter the computational domain at the left and upper boundaries, while particles can exit and be removed from the simulation at any open boundary.

The velocity distribution of particles entering the computational domain (gas molecules in the free stream) follows the Maxwellian distribution function.

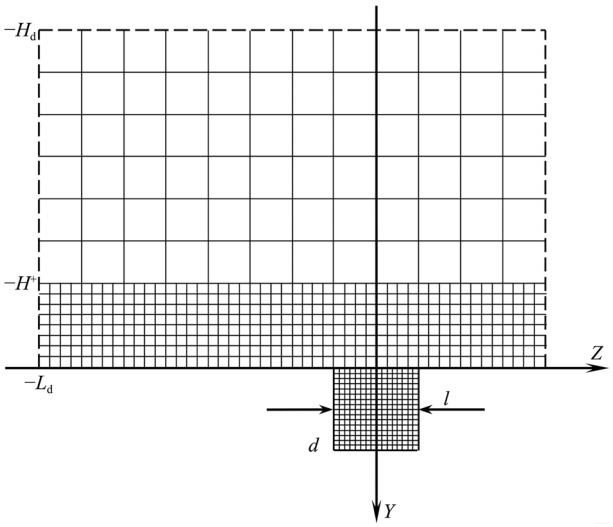

Fig. 2 Computational domain and spatial grid for modeling gas flow over a cavity

$$f(\boldsymbol{v}) = \frac{n_0}{\left(\sqrt{\pi}v_0\right)^3}\exp\left(-\frac{v_x^2 + \left(v_y - U\cdot\sin\alpha\right)^2 + \left(v_z - U\cdot\cos\alpha\right)^2}{v_0^2}\right), \tag{1}$$

where $\boldsymbol{v} = \left(v_x, v_y, v_z\right)$ is the molecular velocity, $v_0 = \sqrt{2kT_0/m}$ is the most probable speed of gas molecules in an equilibrium gas, k is the Boltzmann constant and m is the mass of a gas molecule. The free-stream velocity can be found as follows:

$$U = \sqrt{\gamma/2}\, Ma\, v_0, \tag{2}$$

where $Ma = U/a$ is the free-stream Mach number, $a = \sqrt{\gamma kT_0/m}$ is the speed of sound, and γ is the ratio of specific heat (5/3 for a monatomic gas). In the case of $Ma = 0$, Eq. (1) represents the distribution function of gas molecules crossing a certain plane in an equilibrium gas at temperature T_0 and pressure $P_0 = n_0 kT_0$. When $Ma > 0$, the equilibrium distribution for $Ma = 0$ is first simulated, and then the velocity components v_y and v_z are adjusted by adding values corresponding to the Mach number, $U\sin\alpha$ and $U\cos\alpha$, respectively.

The number of new particles N_+ entering the computational domain through a unit area boundary during the time step Δt is determined by the following expression:

$$N_+ = \left(2\sqrt{\pi}\right)^{-1} n_0 v_0 \left\{\exp\left(-s^2\cos^2\theta + \sqrt{\pi}\, s\,\cos\theta[1 + \mathrm{erf}\,(s\,\cos\theta)]\right)\right\}\Delta t, \tag{3}$$

where $s = U/v_0$ is the molecular velocity ratio, and θ is the angle between the velocity vector of the free stream and the normal vector to the inlet boundary [18]. In our case, $\theta = \alpha$ for the left boundary, and $\theta = \pi/2 - \alpha$ for the upper boundary. In the steady state, the number of particles entering and leaving the computational domain is approximately equal, so the number of particles in the computational domain remains practically constant.

To achieve a steady state (flow), the simulated system was left to evolve on its own for some time, and only after this period from the start of the simulation did the sampling

Table 1 The main simulation parameters: the total number of model particles N, the characteristic size of the computational domain $L_d = H_d$, the cell size Δy, and the time step length Δt

Rarefaction parameter δ	N ($\times 10^6$)	$\frac{L_d}{l}$	$\frac{\Delta y}{l}$	$\frac{\Delta t}{l/(v_0+U)}$
0.01	100	40	1/8	1/10
0.1	100	40	1/8	1/10
1	100	40	1/8	1/10
10	50	10	1/80	1/100
100	50	10	1/80	1/100

(statistics collection) begin. In this study, we used a sufficiently long time interval for this purpose, namely $10\,L_d/l$ in units of l/v_0. This means that if a particle has a velocity v_0 directed along the Y-axis, it can cross the entire simulated system five times during this period. Naturally, this time interval was sufficient to achieve a steady state, as confirmed in all simulations by a zero flow rate through the cavity's inlet section (at the initial moment $t=0$, all particles were located in the region in front of the cavity). The sampling (statistics collection) continued for approximately the same duration.

Significant changes in flow parameters usually occur near the solid boundary (surface), so far from the surface (the value of H^+ was set to be at least $2l$, see Fig. 2), we "coarsened" the grid by increasing the cell size by a factor of 4, while inside the cavity, we reduced the cell size by a factor of 2. The use of the "weighting planes" procedure allows achieving a sufficient number of particles in the cells for correct modeling of intermolecular interactions, and the subdivision of cells into sub-cells ensures that the particles involved in collisions are indeed the closest to each other.

The simulation parameters used in this work include: the number of samples (time steps); the cell size, the time step length and dimensions of the computation domain; the number of model particles in a cell; the time to reach steady flow; and special DSMC procedures—all ensuring a computational error of no more than 1%. Table 1 presents the main simulation parameters, namely the total number of model particles N, the characteristic size of the computational domain $L_d = H_d$, the time step length Δt, and the cell size Δy (at the middle level of the grid).

Let us remind that the set of simulation parameters was chosen in such a way that further improvements (finer spatial grid, shorter time step, etc.) would not lead to changes in the simulation results exceeding the level of computational error. A description of the DSMC procedures and details of the choice of simulation parameters ensuring the specified level of computational error can be found in our previous work [47].

As is commonly accepted in rarefied gas dynamics [17], the rarefaction of the gas will be characterized by the parameter $\delta=(lP_0)/(\mu_0 v_0)$, where μ_0 is the gas viscosity under temperature T_0. In this case, the Knudsen number is inversely proportional to the rarefaction parameter: $Kn = \sqrt{\pi}/(2\delta)$, which for the cavity becomes $Kn=\lambda_0/l$, where λ_0 is the mean free path length of gas molecules in an equilibrium gas at pressure P_0 and temperature T_0. With other necessary similarity criteria, the rarefaction parameter is related to the expression:

$$Re = \sqrt{2\gamma}\, Ma\, \delta, \tag{4}$$

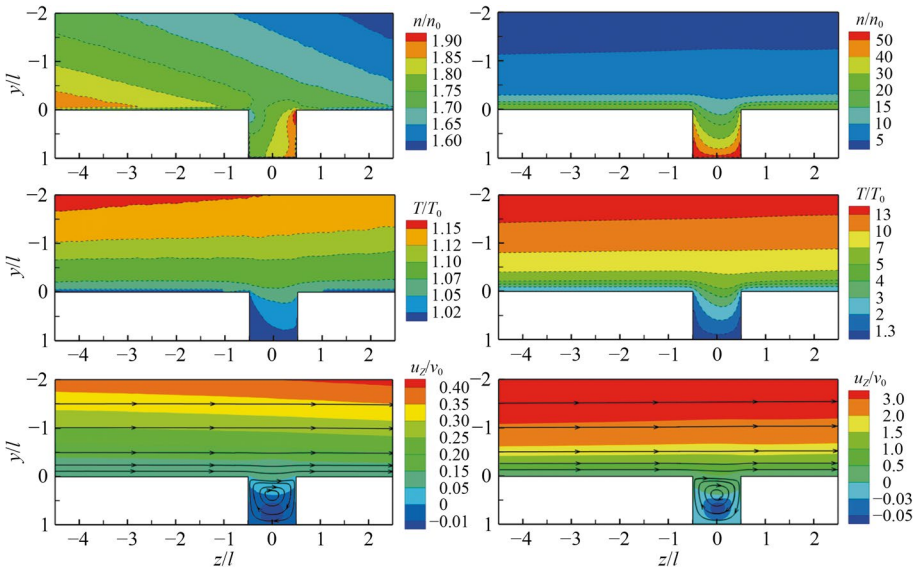

Fig. 3 Dimensionless gas density n/n_0, temperature T/T_0, and longitudinal mass velocity u_Z/v_0 in the YZ-plane both inside the cavity and in the near-region outside the cavity with the length-to-depth ratio $l/d = 1$ at the free-stream Mach numbers $Ma = 1$ (left) and 10 (right) for the rarefaction parameter $\delta = 1$ and the angle of attack $\alpha = 30°$ (the mass velocity images also display gas streamlines)

where $Re = \rho_0 U l/\mu_0$ is the Reynolds number, and $\rho_0 = m\, n_0$ is the mass density of the gas.

One of the calculated characteristics when modeling gas flow in the considered system will be the particle flux density I to the cavity floor. The calculated data will be presented in a dimensionless form $I^* = I/I_0$, where $I_0 = \frac{1}{4} n_0 v_t$ is the particle flux density under free molecular flow conditions $\delta = 0$ at the free-stream Mach number $Ma = 0$, and $v_t = \sqrt{8kT_0/(\pi m)}$ is the mean thermal velocity of gas molecules.

3 Results and discussion

The calculations were carried out over a wide range of gas rarefaction for different values of the cavity length-to-depth ratio l/d, the free-stream Mach number Ma, and the angle of attack α. Figures 3, 4, and other figures in Appendix A show the dimensionless gas density n/n_0, temperature T/T_0, and longitudinal mass velocity u_Z/v_0 in the YZ-plane, both inside the cavity and in the near-region outside the cavity with the length-to-depth ratio $l/d = 1$ at the free-stream Mach numbers $Ma = 1$ and 10 for the rarefaction parameters $\delta = 1$ and 100, and the angles of attack $\alpha = 30°$, 60° and 90°. The mass velocity images also display gas streamlines.

As can be seen from the figures, the distribution of gas macroscopic quantities (flow pattern) depends significantly on all flow parameters Ma, δ and α. Their influence is nontrivial, as it manifests differently depending on the other flow parameters. The change of each flow parameter can lead to both quantitative and qualitative changes in the flow pattern. For example, an increase in the free-stream Mach number Ma not only results in larger values of gas macroscopic quantities but also qualitatively changes the flow pattern. On the other hand, at a fixed angle of attack α and $Ma = 1$, the spatial distributions

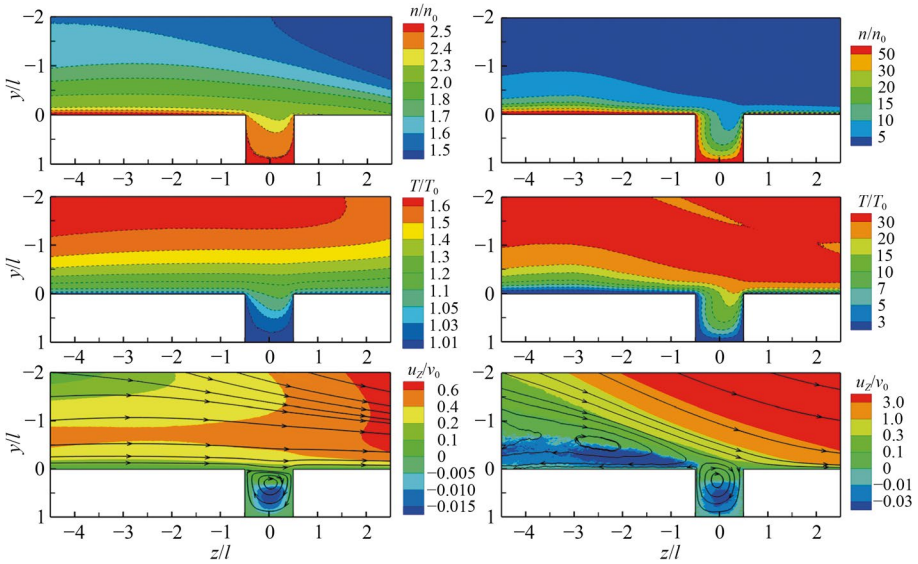

Fig. 4 Dimensionless gas density n/n_0, temperature T/T_0, and longitudinal mass velocity u_Z/v_0 in the YZ-plane both inside the cavity and in the near-region outside the cavity with the length-to-depth ratio l/d=1 at the free-stream Mach numbers Ma= 1 (left) and 10 (right) for the rarefaction parameter $\delta = 100$ and the angle-of-attack α=60° (the mass velocity image also displays gas streamlines)

of density for $\delta = 1$ and $\delta = 100$ are noticeably different; however, the gas density values are approximately in the same numerical range for both $\delta = 1$ and $\delta = 100$.

The value of the angle of attack α significantly determines the flow pattern. As seen in Fig. 3, despite the angle of attack being 30°, the streamlines near the cavity are parallel to the surface (Z-axis). Only at large values of α, such as in Fig. 4 at $\alpha = 60°$, does this parallelism break. Furthermore, Fig. 4 reveals an unexpected fact: at $Ma = 10$, a flow separation zone develops upstream of the cavity, which includes the recirculation zone and the reverse flow zone. It is interesting to note that in this case, the cavity itself also partially participates in the reverse flow. However, the question remains: what exactly is the observed effect? If the computational domain significantly increases, particularly the longitudinal size L_d, will the cavity still participate in the reverse flow? But this is beyond the scope of the present article and requires additional calculations. Directly inside the cavity itself, as seen in the figures for $\alpha = 30°$ and 60°, a single vortex forms, and at $\delta = 1$ its shape depends only weakly on the flow parameters.

At $\alpha = 90°$, as expected, outside the cavity the streamlines are symmetrical with respect to the central line of the cavity $Z = 0$ (Figs. 10 and 12 in Appendix A), while inside the cavity, as seen from these figures, the gas is almost motionless. Therefore, it is difficult to determine streamlines inside the cavity using the DSMC method, as it is not efficient for low-speed gas flow calculations. For these calculations, it is more appropriate to use other methods, such as the discrete velocity method (DVM). Indeed, Naris and Valougeorgis, using DVM to solve the linearized Bhatnagar-Gross-Krook (BGK) model of the Boltzmann equation, were able to accurately calculate even secondary eddies in low-speed cavity flow [48]. However, as the authors themselves note, their study has a number of limitations.

Figure 5 and other figures in Appendix B. show the vertical distributions of density n/n_0, temperature T/T_0, and mass velocity component u_Y/v_0 in the modeled system with

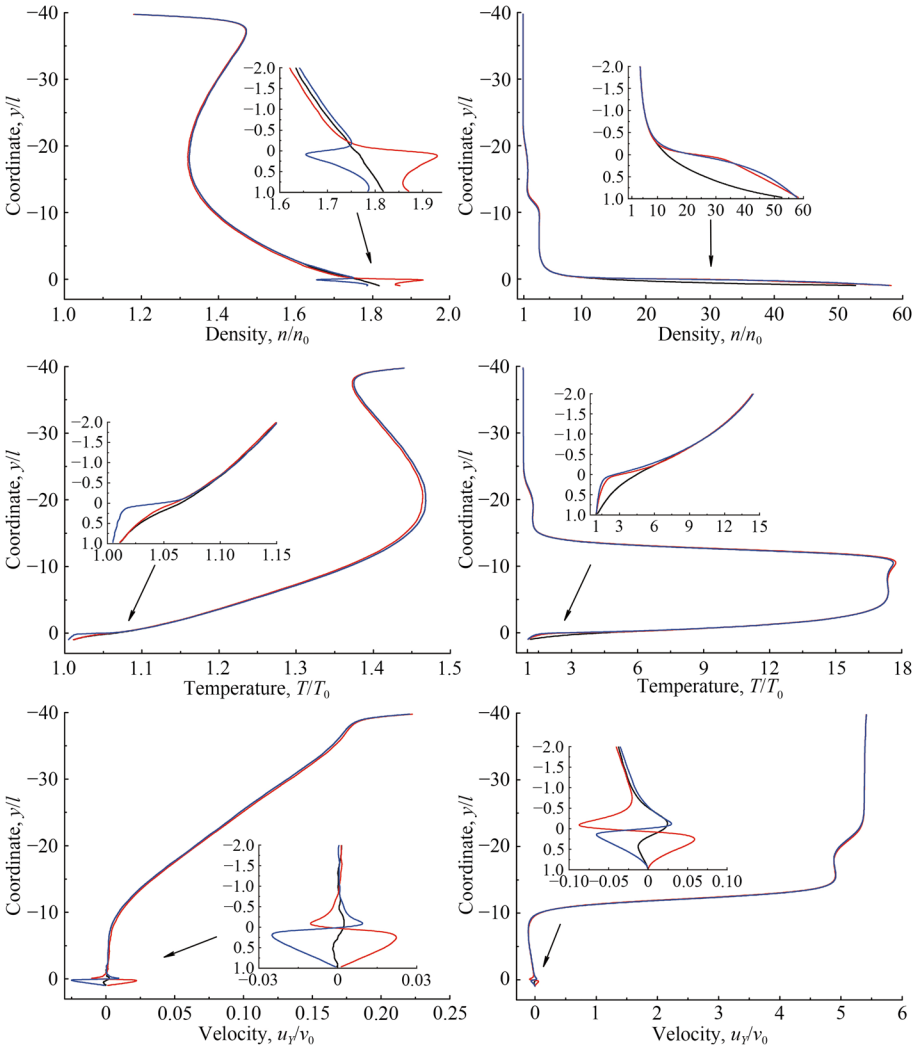

Fig. 5 Vertical distributions of density n/n_0, temperature T/T_0, and mass velocity component u_Y/v_0 in the modeled system with the cavity length-to-depth ratio $l/d = 1$ along lines $z/l = 0$ (black), $z/l = 0.5$ (red) and $z/l = -0.5$ (blue) at the free-stream Mach numbers $Ma = 1$ (left) and 10 (right) for the rarefaction parameter $\delta = 1$ and the angle of attack $\alpha = 30°$

the cavity length-to-depth ratio $l/d = 1$ along lines $z/l = 0$, $z/l = 0.5$, and $z/l = -0.5$ at the angles of attack $\alpha = 30°$, 60° and 90° for the free-stream Mach numbers $Ma = 1$ and 10, and the rarefaction parameters $\delta = 1$ and 100. In the case of $y > 0$ (see Figs. 1 and 2), these figures represent distributions inside the cavity, namely along the centerline ($z/l = 0$), the right wall ($z/l = 0.5$), and the left wall ($z/l = -0.5$) of the cavity. In each figure, such distributions are presented in an inset with an enlarged scale.

As shown in these figures, particularly in Fig. 5, the difference in vertical distributions of gas macroscopic quantities along $z/l = 0$, $z/l = 0.5$ and $z/l = -0.5$ is primarily observed near and inside the cavity, especially in the distribution of the mass velocity component u_Y/v_0. Specifically, as seen in Fig. 5, inside the cavity, the value of u_Y/v_0 takes positive values along the right wall ($z/l = 0.5$) and negative values along the left wall ($z/l = -0.5$), which indicates a clockwise circulation of the gas, as also confirmed by the image in Fig. 3.

It can also be observed from Fig. 5 and other figures in Appendix B. that for a free-stream Mach number $Ma = 10$, near the floor of the cavity, the density ratio n/n_0 can reach double- and even triple-digit values, in contrast to the temperature ratio T/T_0 and the mass velocity component u_Y/v_0, whose values approach those for undisturbed gas, i.e., 1 and 0, respectively. This indicates that, at $Ma = 10$, there is highly compressed but not heated, and relatively slow-moving gas near the cavity floor.

Figure 5 and other figures in Appendix B. show that at a certain distance from the cavity's inlet section, an abrupt change in the gas macroscopic quantities is observed. This is particularly pronounced at the free-stream Mach number $Ma = 10$ and the rarefaction parameter $\delta = 100$. Such an abrupt change in macroscopic quantities indicates that the gas flow passes through a so-called detached shock. The more intense the shock, the greater the reduction in flow velocity and the increase in gas density and temperature behind it. The figures demonstrate that the intensity and localization of the shock depend on both the free-stream Mach number Ma and the rarefaction parameter δ. The higher the flow velocity and the denser the gas, the more abrupt and significant the changes in gas macroscopic quantities, and the closer the shock is located to the cavity's inlet section.

It should be recalled that such detached shocks occur due to the interaction of a supersonic gas flow with the surface of a solid body, when the flow regime transitions from supersonic to subsonic. Upstream of the shock, the supersonic flow remains undisturbed, approaching the shock "blindly". Within the shock region, abrupt changes occur in the gas macroscopic quantities, such as density, temperature, and mass velocity. Specifically, in the shock, the supersonic velocity abruptly transitions to subsonic. As the gas flow passes through the shock, a qualitative change in its energy takes place: part of the kinetic energy is converted into thermal (internal) energy. The total energy of the flow before and after the shock remains constant. However, behind the shock, the flow possesses less kinetic energy and more thermal energy. As a result, a region of compressed and heated gas with subsonic velocities forms in front of the body. Thus, the shock acts as a boundary between two regions of gas with different macroscopic quantities: one supersonic and the other subsonic.

Figure 5 and other figures in Appendix B. also indicate that detached shocks at $\alpha = 30°$ and 60° exhibit a more complex structure than the shock at $\alpha = 90°$. A complete 2D representation of the latter can be found in our previous work [45]. Here, we present only the dimensionless gas density n/n_0 and the gas streamlines in the YZ-plane for the modeled system with a cavity length-to-depth ratio of $l/d = 1$, at the free-stream Mach number $Ma = 10$, the rarefaction parameter $\delta = 10$, and the angle of attack $\alpha = 90°$ (see Fig. 6). As shown in the figure, a detached shock forms at a distance of approximately $4l$ from the cavity's inlet section, where the gas streamlines abruptly change direction. A detailed investigation of the detached shock structure requires a separate study, which is beyond the scope of this article. However, it is worth noting that it would be reasonable to examine the structure of the detached shock by modeling the attack of a high-speed rarefied gas flow on a free surface, particularly one without cavities or channels, so that these elements do not distort the flow field.

In Table 2, the results of the calculation of the dimensionless particle flux density I^* to the cavity floor are presented as a function of the rarefaction parameter δ, the angle of

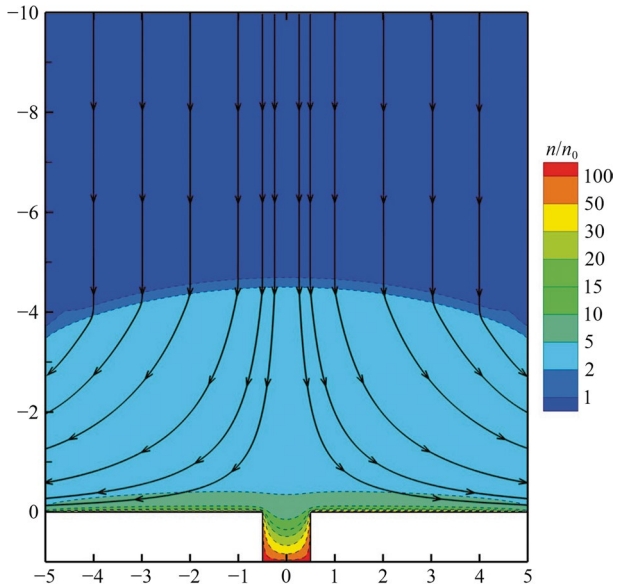

Fig. 6 Dimensionless gas density n/n_0 and gas streamlines in the *YZ*-plane for the modeled system with the cavity length-to-depth ratio l/d=1, at the free-stream Mach number Ma= 10, the rarefaction parameter δ = 10, and angle of attack $\alpha = 90°$

Table 2 The dimensionless particle flux density I^* to the cavity floor as a function of the rarefaction parameter δ, the angle of attack α and the free-stream Mach number Ma for the length-to-depth ratio $l/d = 1$

Ma	***α* (°)**	**Particle flux density I^***				
		$\delta = 0.01$	**0.1**	**1**	**10**	**100**
1	30	2.07	1.87	1.82	1.94	1.99
	60	3.27	2.64	2.38	2.45	2.51
	90	4.08	3.23	2.79	2.80	2.78
10	30	23.3	50.4	58.1	56.7	54.3
	60	63.9	116	148	150	137
	90	73.4	141	159	160	n/d

attack α, and the free-stream Mach number Ma for the length-to-depth ratio $l/d = 1$. For the case with flow parameters $Ma = 10$, $\alpha = 90°$ and $\delta = 100$, the results could not be obtained due to the unacceptably large computation time. As can be seen from the table, for a fixed angle of attack α, in the case of a highly rarefied gas ($\delta = 0.01$) at $Ma = 1$, the maximum value of I^* is observed, while at $Ma = 10$, on the contrary, this case ($\delta = 0.01$) corresponds to the minimum value of I^*.

At the free-stream Mach number $Ma = 1$, in the transitional flow regime at $\delta = 1$, a minimum in the value of I^* is observed, at least for $\alpha = 30°$ and 60°. It is interesting to note that in the transitional regime at the same value of δ, the minimum in the flow rate (Knudsen paradox) is observed when a rarefied gas flows through sufficiently long channel. For $\alpha = 90°$, the value of I^* reaches its minimum at $\delta = 1$, and then, with an increase in δ, it no longer changes. At the free-stream Mach number $Ma = 10$, the dependence of the particle flux density I^* on the rarefaction parameter δ is non-trivial, and it is difficult to identify any clear trend.

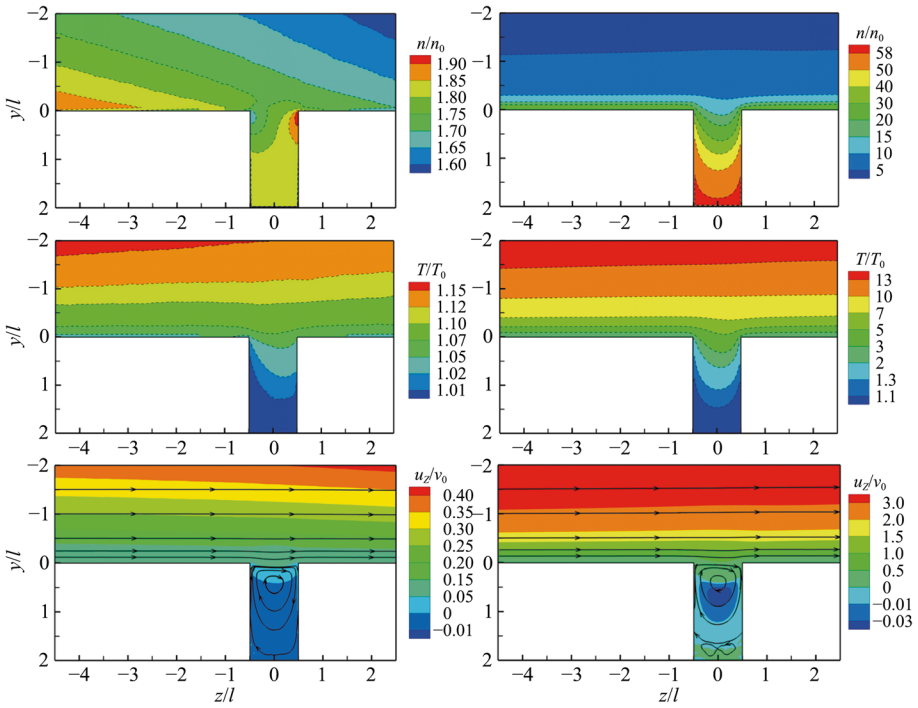

Fig. 7 Dimensionless gas density n/n_0, temperature T/T_0, and longitudinal mass velocity u_Z/v_0 in the YZ-plane both inside the cavity and in the near-region outside the cavity with the length-to-depth ratio $l/d = 0.5$ at the free-stream Mach numbers $Ma = 1$ (left) and 10 (right) for the angle of attack $\alpha = 30°$ and the rarefaction parameter $\delta = 1$ (the mass velocity image also displays gas streamlines)

Completing the discussion, let's consider the dependence of gas macroscopic quantities on the geometric dimensions of the cavity. According to the horizontal pressure distribution along the cavity floor, high-speed gas flow over a cavity can be divided into three types: open, closed, and transitional [49]. In the case of closed flow, the free-stream is divided in such a way that recirculation zones appear in the corners of the cavity, and in the central region, the free-stream reaches the cavity floor, so the pressure distribution along the cavity floor is significantly non-uniform. In the case of open flow, a single vortex forms inside the cavity, which covers the entire cavity, leading to a nearly uniform pressure distribution along the cavity floor, with only a slight increase at the downstream corner of the cavity. The boundaries between the different types of flow were established as follows [50]: open cavity flow occurs for cavities with a length-to-depth ratio $l/d \leq 10$; closed cavity flow occurs for shallow cavities with $l/d > 13$; transitional flow occurs between the boundaries of open and closed flow. It was later found that the boundaries are not only dependent on the l/d ratio but also on the free-stream Mach number Ma and the cavity width-to-depth ratio w/d [51]. In our opinion, the angle of attack α and gas rarefaction δ should also be considered as governing parameters, although a strict justification for this requires additional research.

Figures 7, 8 and other figures in Appendix C. show the dimensionless gas density n/n_0, temperature T/T_0, and longitudinal mass velocity u_Z/v_0 in the YZ-plane both inside the cavity and in the near-region outside the cavity with the length-to-depth ratio $l/d = 0.5$ and 2 at the angle of attack $\alpha = 30°$, 60°, and 90° for the free-stream Mach numbers Ma

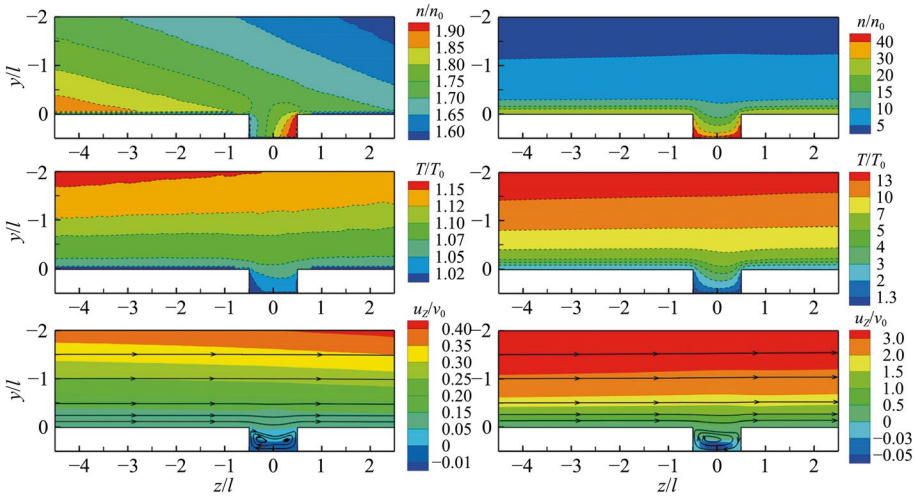

Fig. 8 Dimensionless gas density n/n_0, temperature T/T_0, and longitudinal mass velocity u_Z/v_0 in the *YZ*-plane both inside the cavity and in the near-region outside the cavity with the length-to-depth ratio $l/d = 2$ at the free-stream Mach numbers $Ma = 1$ (left) and 10 (right) for the angle of attack $\alpha = 30°$ and the rarefaction parameter $\delta = 1$ (the mass velocity image also displays gas streamlines)

$= 1$ (left) and 10 (right) in the case of the rarefaction parameter $\delta = 1$ (the mass velocity images also display gas streamlines). According to the classification [50], the presented 2D cavity flow patterns correspond to the open flow. Indeed, for a cavity with $l/d = 0.5$, the density and temperature distributions along the floor appear uniform. However, as seen in Fig. 8, in a cavity with $l/d = 2$ at $Ma = 1$, the transition from open flow to closed flow is already noticeable. Specifically, the density distribution along the floor becomes significantly non-uniform, and the gas streamlines begin to form the pattern of closed cavity flow. Thus, the circulation pattern of the flow inside the cavity is largely determined by its geometric size l/d. The circulation patterns obtained in this study are consistent with and do not contradict previous research, particularly [22, 23, 32].

Table 3 shows the calculation results of the dimensionless particle flux density I^* to the cavity floor as a function of the length-to-depth ratio l/d and the angle of attack α for the free-stream Mach numbers $Ma = 1$ and 10, and for the rarefaction parameters $\delta =$ 1 and 100. As shown in the table, at $Ma = 1$, for fixed values of α and δ, the particle flux

Table 3 The dimensionless particle flux density I^* to the cavity floor as a function of the length-to-depth ratio l/d and the angle of attack α for the free-stream Mach numbers $Ma = 1$ and 10, and for the rarefaction parameters $\delta = 1$ and 100

Ma	α (°)	Particle flux density I^*					
		$\delta = 1$			$\delta = 100$		
		$l/d = 0.5$	1	2	$l/d = 0.5$	1	2
1	30	1.83	1.82	1.82	1.99	1.99	1.99
	60	2.39	2.38	2.37	2.51	2.51	2.51
	90	2.81	2.79	2.77	2.78	2.78	2.78
10	30	59.3	58.11	55.1	52.2	54.3	54.5
	60	150	148	141	138	137	136
	90	162	159	152	n/d	n/d	n/d

density I^* is independent of the length-to-depth ratio l/d, as the results coincide within the computational error. At $Ma = 10$, the results are close to each other, but the discrepancy exceeds the computational error. Only for the flow parameters $Ma = 10$, $\alpha = 60°$, and $\delta = 100$, it can be asserted that I^* is independent of l/d.

4 Concluding remarks

The direct simulation Monte Carlo (DSMC) method was used to investigate the high-speed gas flow over a cavity at different angles of attack over a wide range of gas rarefaction. Calculations were performed for cavity length-to-depth ratios $l/d = 0.5$, 1 and 2; for angles of attack $\alpha = 30°$, 60°, and 90°; and for the free-stream Mach numbers $Ma = 1$ and 10, with the rarefaction parameter δ ranging from 0.01 to 100.

The main results of the study are as follows:

- 2D flow field patterns, including the dimensionless density, temperature, and longitudinal mass velocity of the gas, as well as gas streamlines both inside and outside the cavity;
- Vertical 1D distributions of the gas macroscopic quantities within the modeled system;
- The values of the dimensionless particle flux density to the cavity floor.

It was established that the flow field strongly depends on all flow parameters Ma, δ, and α. Their influence is nontrivial, as it manifests differently depending on the other flow parameters. Changes in each flow parameter can result in both quantitative and qualitative changes in the distribution of gas macroscopic quantities.

The influence of the geometric dimensions l/d showed that the flow field in all the studied cavities corresponds to an open flow regime. However, in the shallow cavity with $l/d = 2$ at $Ma = 1$ and $\delta = 1$, the transition from open flow to closed flow has already begun.

The dimensionless particle flux density I^* to the cavity floor depends primarily on the parameters Ma and α, rather than δ, and it is practically independent of l/d. Similar to the Knudsen paradox observed in the transitional flow regime, for $Ma = 1$, a minimum value of I^* was found at $\delta = 1$.

At a certain distance from the cavity, the gas flow passes through a detached shock, where the flow regime transitions from supersonic to subsonic. The intensity and location of the shock depend on both the free-stream Mach number Ma and the rarefaction parameter δ. The higher the flow velocity and the denser the gas, the more abrupt and significant the changes in the gas macroscopic quantities, and the closer the shock is located to the cavity's inlet section. Detached shocks at angles of attack $\alpha = 30°$ and 60° exhibit more complex structures than at $\alpha = 90°$.

In the immediate vicinity of the cavity inlet, a complex flow structure may develop. In particular, for the flow parameters $Ma = 10$, $\alpha = 60°$, and $\delta = 100$, a flow separation zone

forms upstream of the cavity with $l/d = 1$, including both gas recirculation and a reverse flow.

Inside the cavity, at angles of attack $\alpha = 30°$ and 60°, a single vortex forms, the shape of which depends weakly on the flow parameters, at least at $\delta = 1$ for a cavity with $l/d = 1$. At $\alpha = 90°$, outside the cavity, the streamlines are symmetrical relative to the cavity's centerline, while inside the cavity, the gas remains almost motionless.

The results obtained provide valuable insights into the relationship between flow parameters such as Mach number, rarefaction, and angle of attack, and their impact on the flow structure over a cavity. The results can be applied to optimize the aerodynamic performance of systems operating in rarefied gas conditions, such as hypersonic vehicles and spacecraft. Of particular importance is the understanding of the transition from supersonic to subsonic flow in the form of detached shocks, which is critical for improving the aerodynamic efficiency of cavities. Future research could expand on this by considering additional characteristics, such as cavity shape, gas molecule–molecule interaction, and gas-surface scattering, for more accurate predictions.

Appendix A

Dimensionless gas density n/n_0, temperature T/T_0, and longitudinal mass velocity u_Z/v_0 in the YZ-plane both inside the cavity and in the near-region outside the cavity with the length-to-depth ratio $l/d = 1$ at the free-stream Mach numbers $Ma = 1$ (left) and 10 (right). The mass velocity images also display gas streamlines.

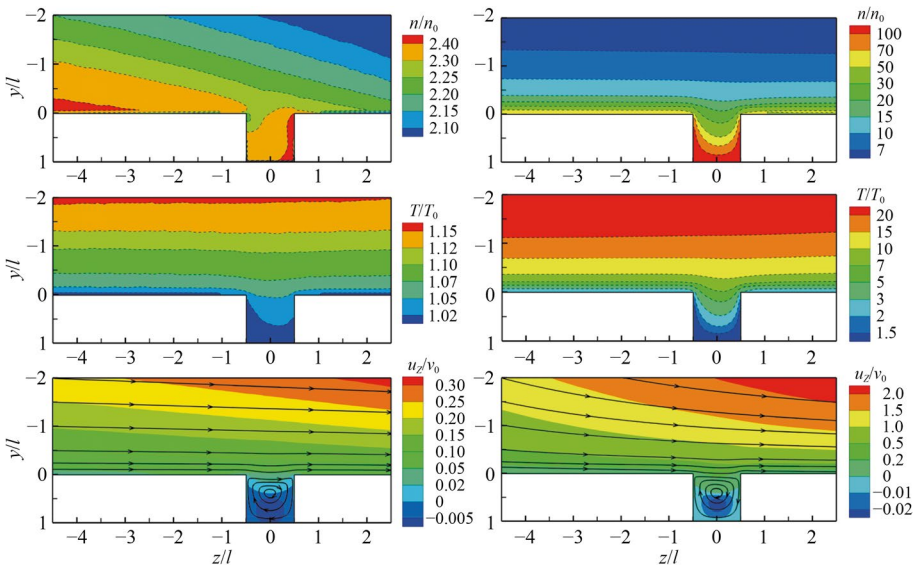

Fig. 9 Images for the rarefaction parameter $\delta = 1$ and the angle of attack $\alpha = 60°$

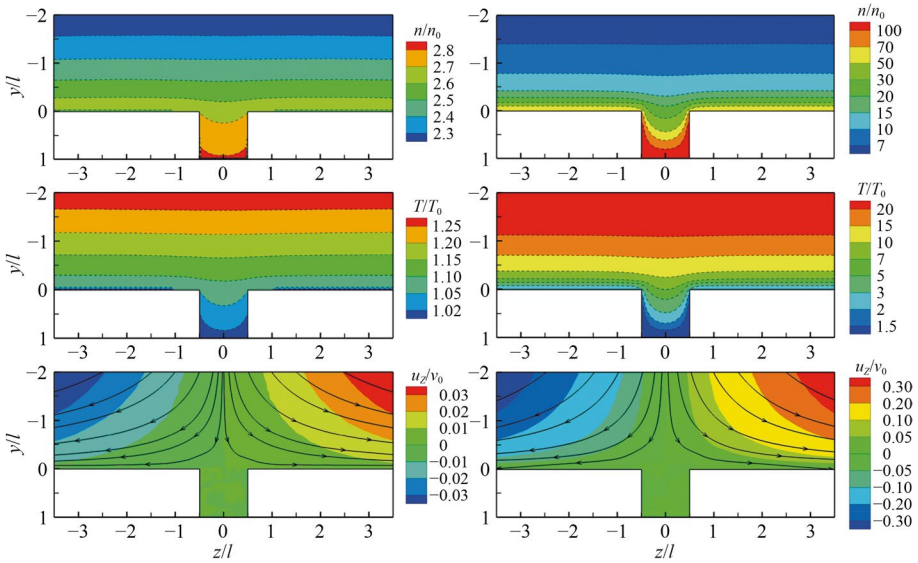

Fig. 10 Images for the rarefaction parameter $\delta = 1$ and the angle of attack $\alpha = 90°$

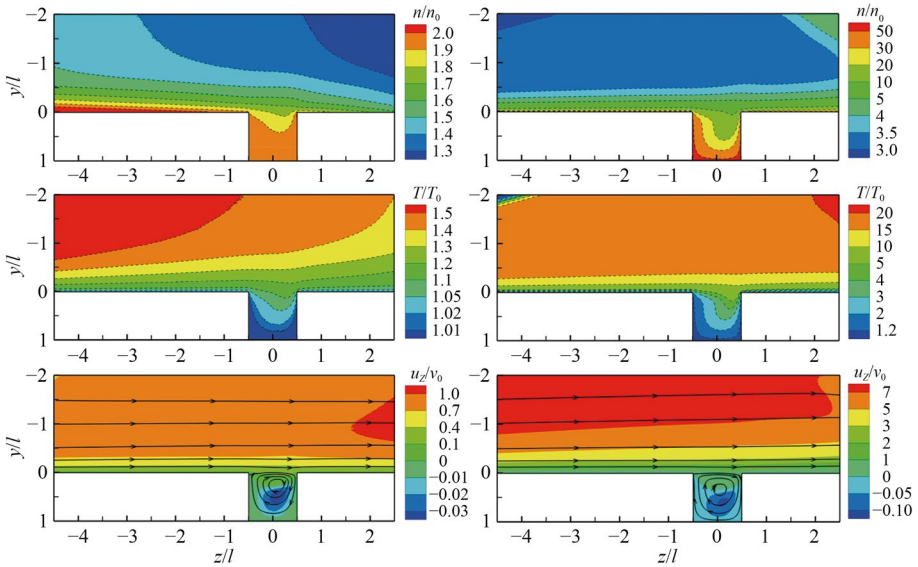

Fig. 11 Images for the rarefaction parameter $\delta = 100$ and the angle of attack $\alpha = 30°$

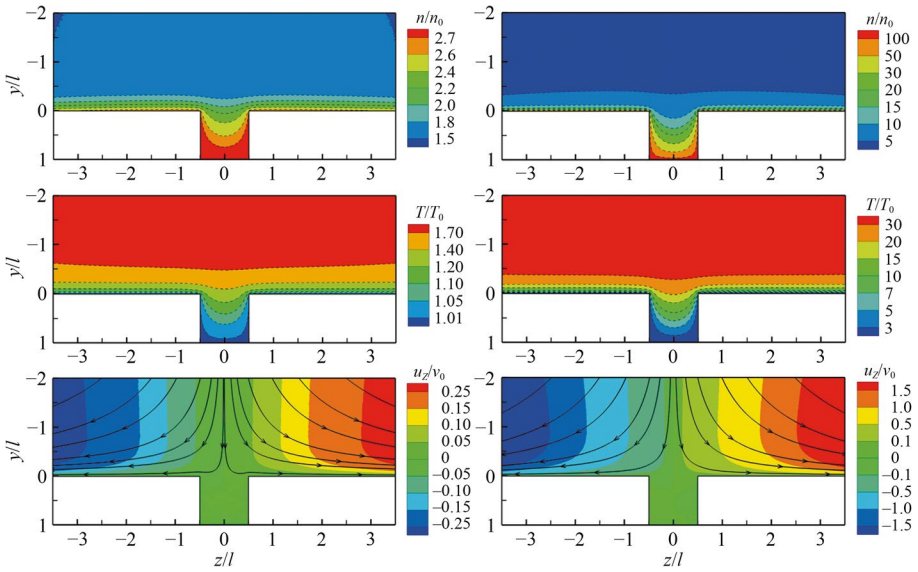

Fig. 12 Images for the rarefaction parameter $\delta = 100$ (left) and $\delta = 10$ (right), and the angle of attack $\alpha = 90°$

Appendix B

Vertical distributions of density n/n_0, temperature T/T_0, and mass velocity component u_Y/v_0 in the modeled system with the cavity length-to-depth ratio $l/d = 1$ along lines $z/l = 0$ (black), $z/l = 0.5$ (red) and $z/l = -0.5$ (blue) at the free-stream Mach numbers $Ma = 1$ (left) and 10 (right).

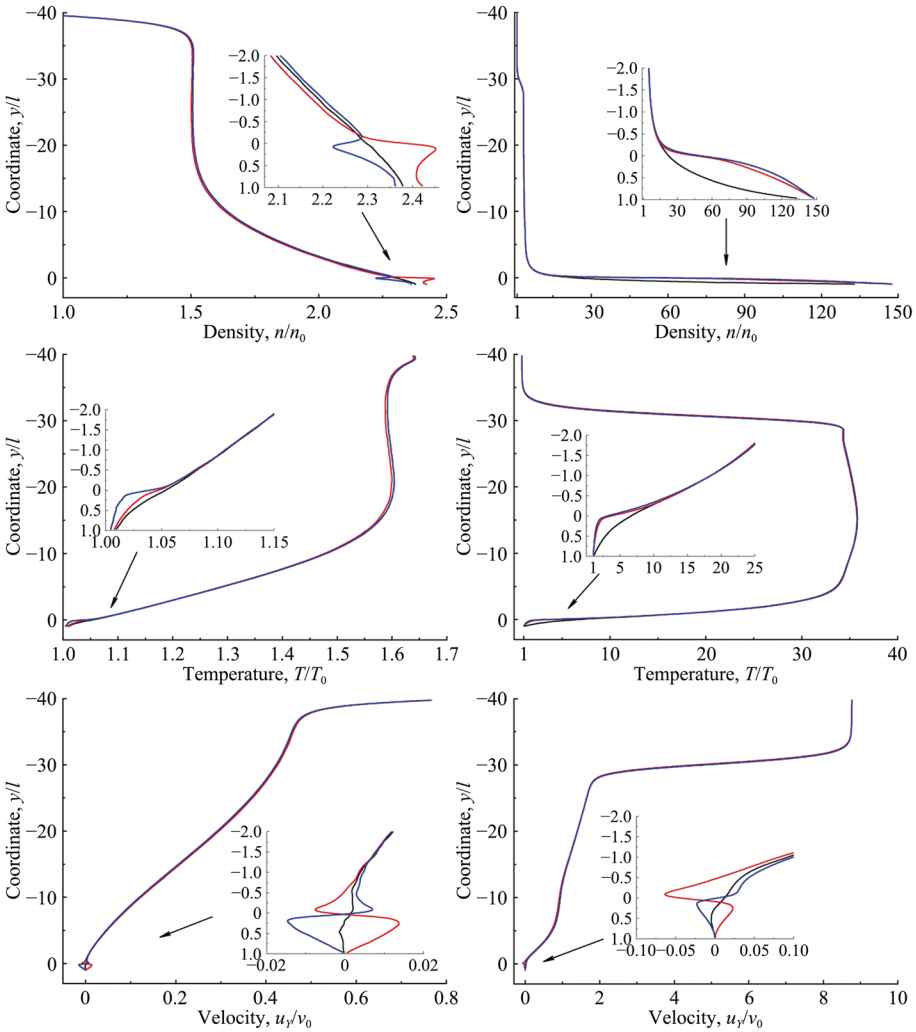

Fig. 13 Images for the rarefaction parameter $\delta = 1$ and the angle of attack $\alpha = 60°$

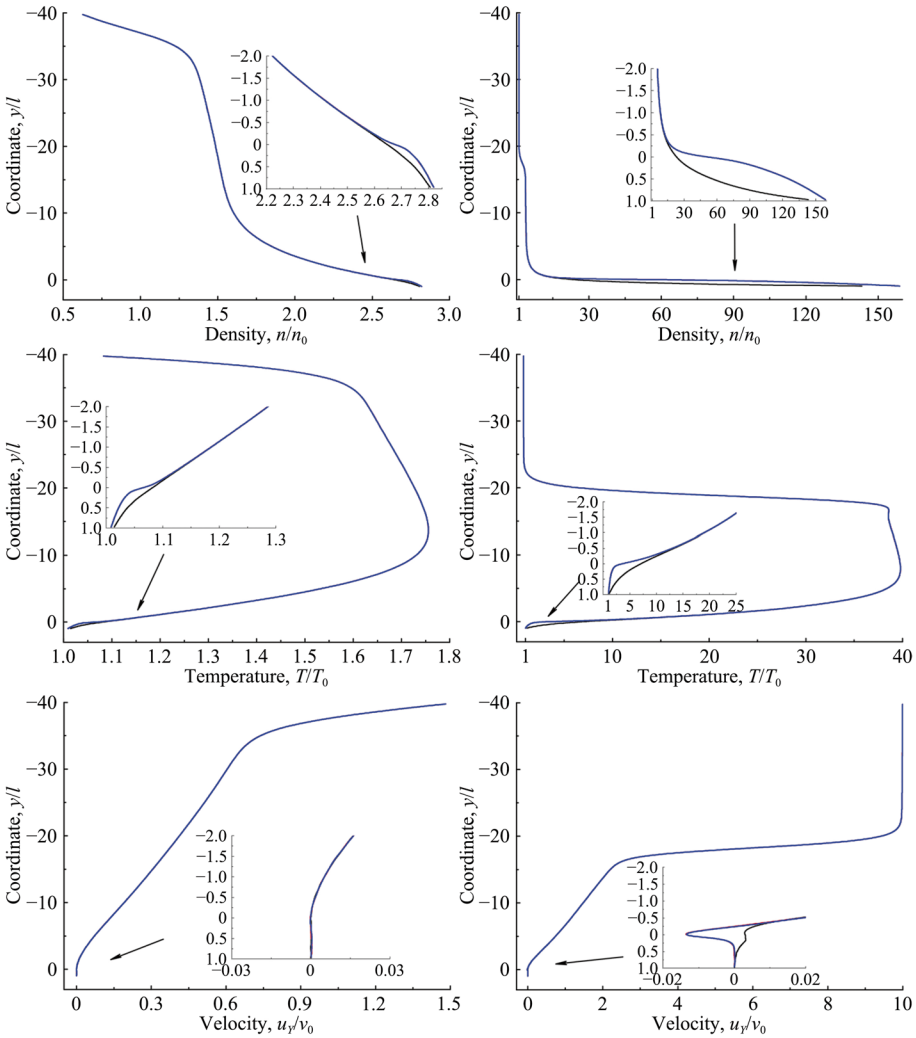

Fig. 14 Images for the rarefaction parameter $\delta = 1$ and the angle of attack $\alpha = 90°$

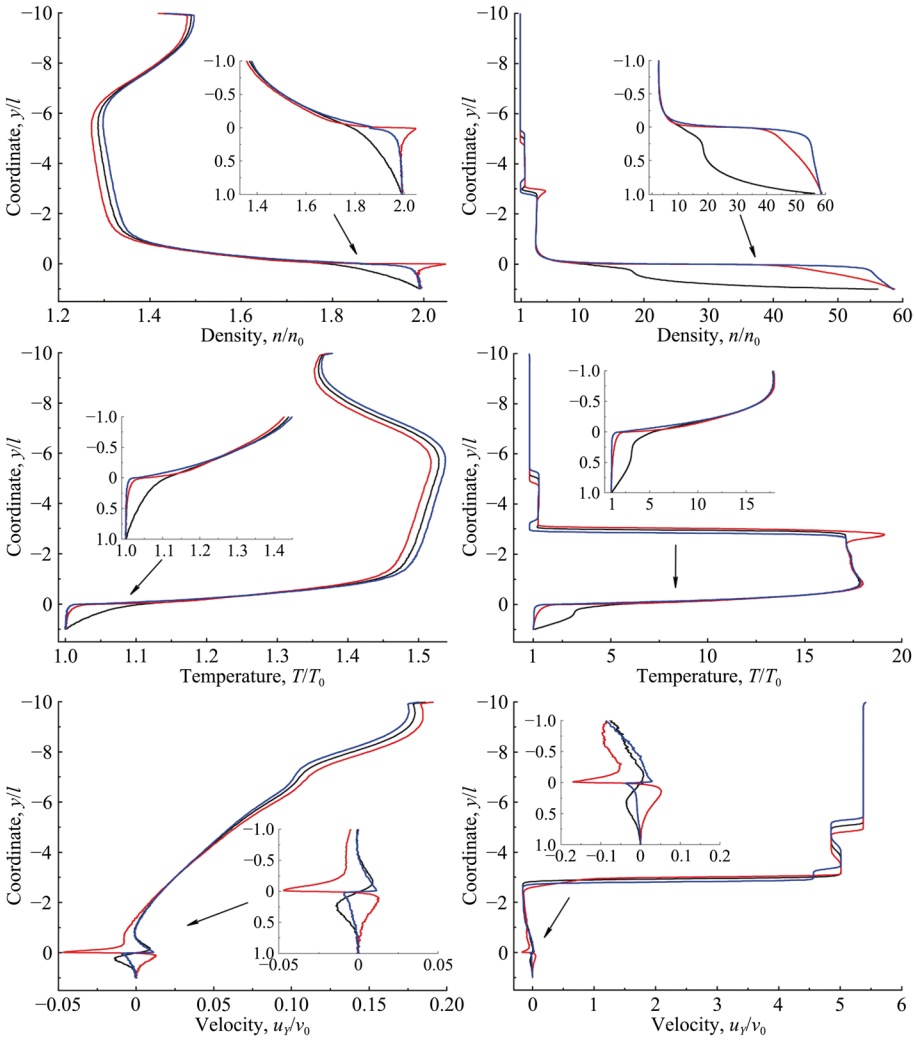

Fig. 15 Images for the rarefaction parameter $\delta = 100$ and the angle of attack $a = 30°$

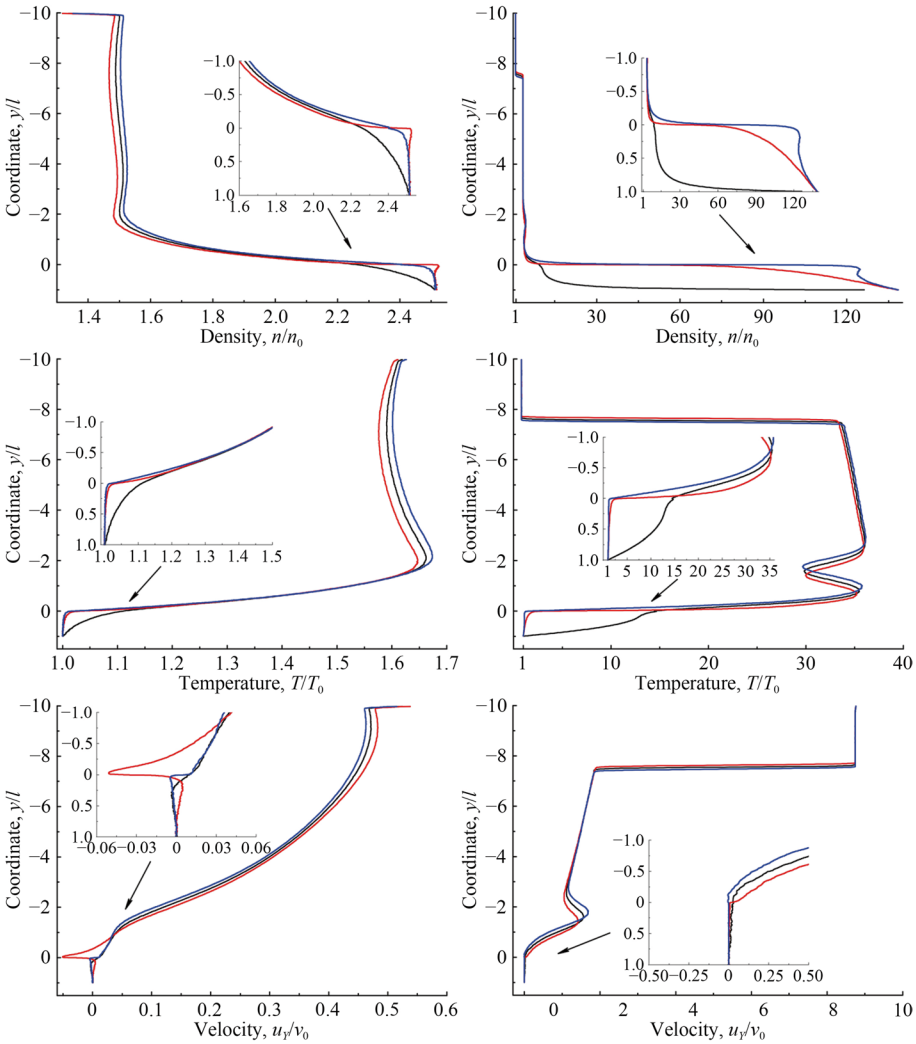

Fig. 16 Images for the rarefaction parameter $\delta = 100$ and the angle of attack $\alpha = 60°$

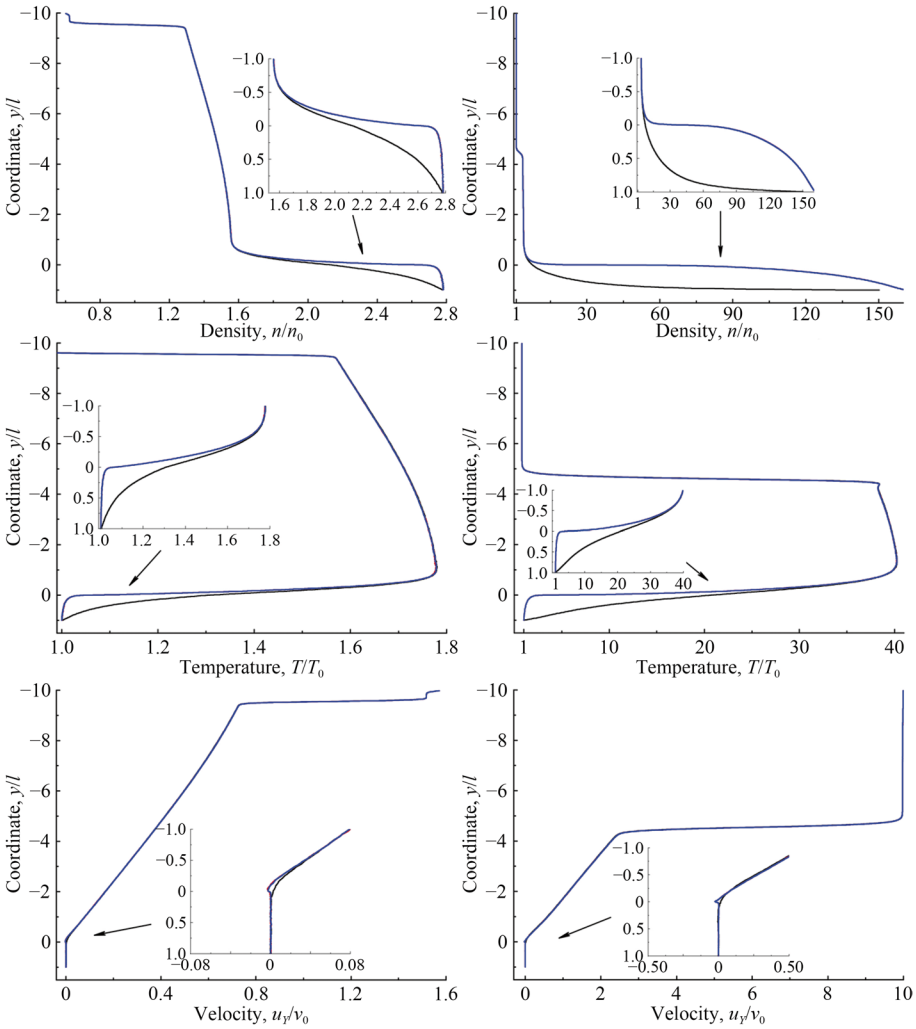

Fig. 17 Images for the rarefaction parameter $\delta = 100$ (left) and $\delta = 10$ (right), and the angle of attack $\alpha = 90°$

Appendix C

Dimensionless gas density n/n_0, temperature T/T_0, and longitudinal mass velocity u_Z/v_0 in the YZ-plane both inside the cavity and in the near-region outside the cavity at the free-stream Mach numbers $Ma = 1$ (left) and 10 (right) in the case of the rarefaction parameter $\delta = 1$. The mass velocity images also display gas streamlines.

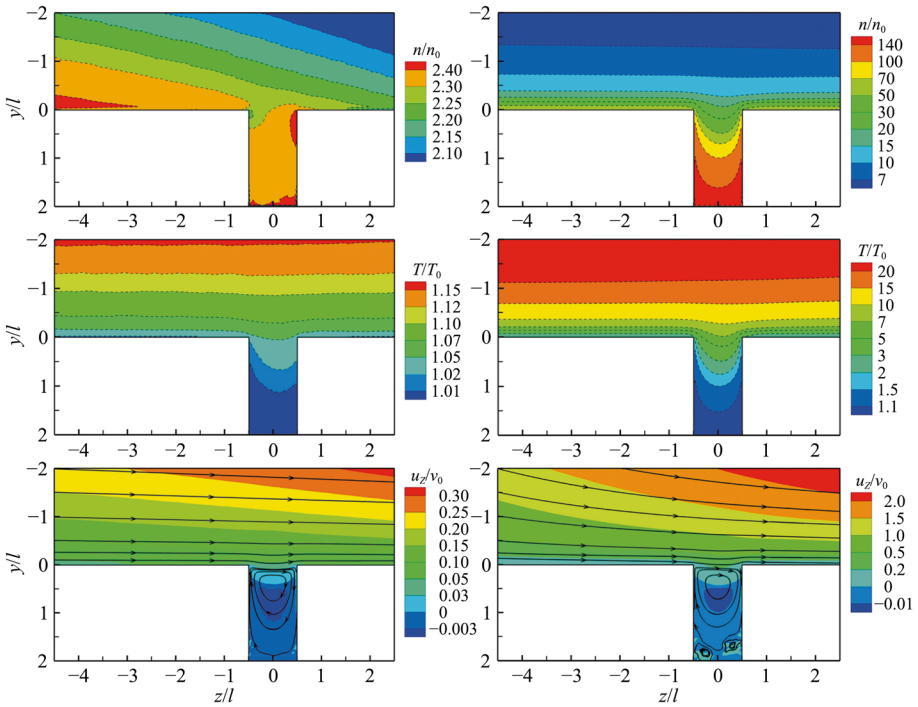

Fig. 18 Images for the length-to-depth ratio $l/d = 0.5$ and the angle of attack $\alpha = 60°$

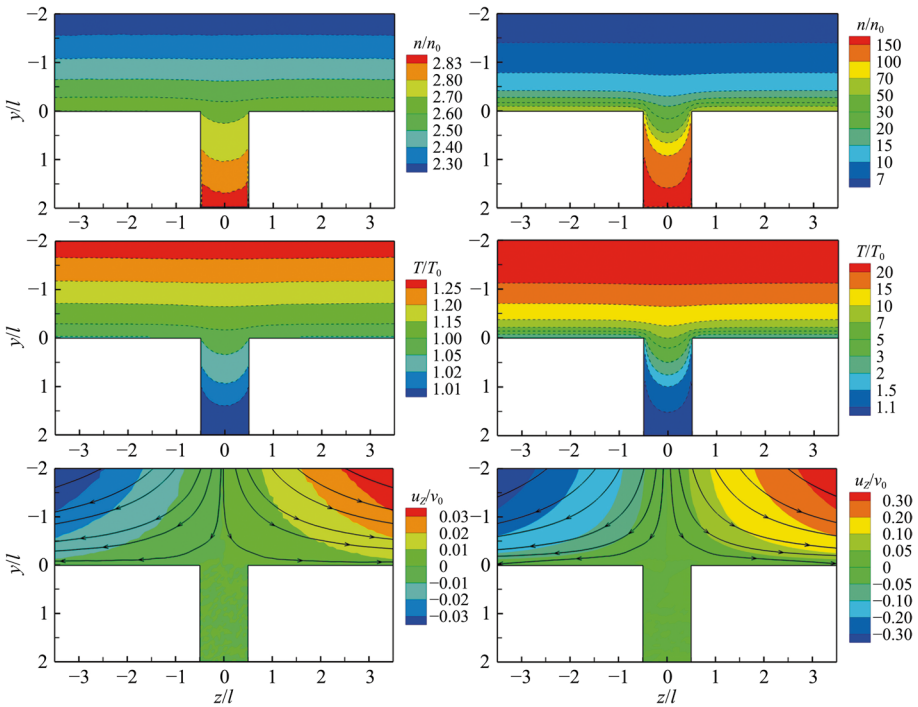

Fig. 19 Images for the length-to-depth ratio $l/d = 0.5$ and the angle of attack $\alpha = 90°$

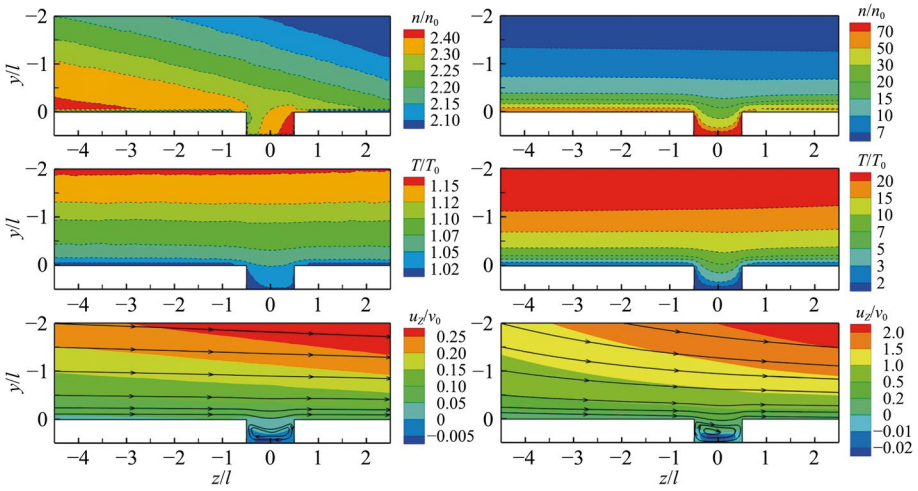

Fig. 20 Images for the length-to-depth ratio $l/d = 2$ and the angle of attack $\alpha = 60°$

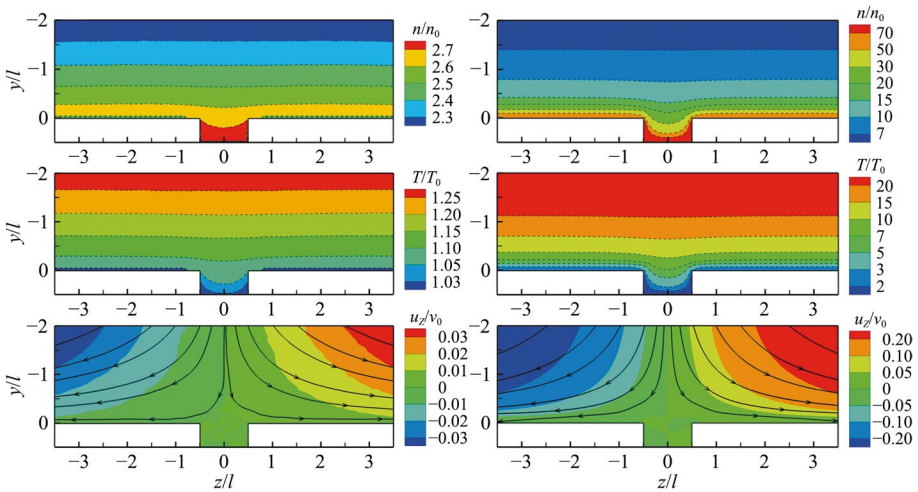

Fig. 21 Images for the length-to-depth ratio $l/d = 2$ and the angle of attack $\alpha = 90°$

Acknowledgements
Not applicable.

Authors' contributions
OS is the sole author of the article. The author has read and approved the final manuscript.

Funding
This research was supported by the Ministry of Education and Science of the Russian Federation under the state contract with Higher Education Institutions (research project FEUZ-2023–0022).

Data availability
Data will be made available on reasonable request.

Declarations

Competing interests
The author declares that no financial or personal relationships that may be perceived as influencing this work.

Received: 19 December 2024 Revised: 25 February 2025 Accepted: 18 March 2025
Published online: 14 February 2026

References

1. Anderson JD Jr, Cadou CP (2024) Fundamentals of aerodynamics, 7th edn. McGraw-Hill, New York
2. Lawson SJ, Barakos GN (2011) Review of numerical simulations for high-speed, turbulent cavity flows. Prog Aerosp Sci 47(3):186–216. https://doi.org/10.1016/j.paerosci.2010.11.002
3. Wang ZG, Sun XW, Huang W et al (2016) Experimental investigation on drag and heat flux reduction in supersonic/hypersonic flows: A survey. Acta Astronaut 129:95–110. https://doi.org/10.1016/j.actaastro.2016.09.004
4. Sun X, Huang W, Ou M et al (2019) A survey on numerical simulations of drag and heat reduction mechanism in supersonic/hypersonic flows. Chin J Aeronaut 32(4):771–784. https://doi.org/10.1016/j.cja.2018.12.024
5. Sazhin O (2023) Gas dynamics of micro- and nanofluidic systems. Fluids 8(1):24. https://doi.org/10.3390/fluids8010024
6. Charwat AF, Roos JN, Dewey FC Jr et al (1961) An investigation of separated flows-Part I: The pressure field. J Aerosp Sci 28(6):457–470. https://doi.org/10.2514/8.9037
7. Charwat AF, Dewey CF Jr, Roos JN et al (1961) An investigation of separated flows-Part II: Flow in the cavity and heat transfer. J Aerosp Sci 28(7):513–527. https://doi.org/10.2514/8.9099
8. Nestler DE, Saydah AR, Auxer WL (1969) Heat transfer to steps and cavities in hypersonic turbulent flow. AIAA J 7(7):1368–1370. https://doi.org/10.2514/3.5351
9. Tracy MB, Plentovich EB (1993) Characterization of cavity flow fields using pressure data obtained in the Langley 0.3-meter transonic cryogenic tunnel (NASA Technical Memorandum 4436). National Aeronautics and Space Administration, Hampton
10. Zhang J, Morishita E, Okunuki T et al (2001) Experimental and computational investigation of supersonic cavity flows. In: 10th AIAA/NAL-NASDA-ISAS International Space Planes and Hypersonic Systems and Technologies Conference, Kyoto, 24-27 April 2001. https://doi.org/10.2514/6.2001-1755
11. Jackson AP, Hillier R, Soltani S (2001) Experimental and computational study of laminar cavity flows at hypersonic speeds. J Fluid Mech 427:329–358. https://doi.org/10.1017/S0022112000002433
12. Everhart JL, Alter SJ, Merski NR et al (2006) Pressure gradient effects on hypersonic cavity flow heating. In: 44th AIAA Aerospace Sciences Meeting and Exhibit, Reno, 9-12 January 2006. https://doi.org/10.2514/6.2006-185
13. Horvath TJ, Berry SA, Merski NR et al (2006) Shuttle damage/repair from the perspective of hypersonic boundary layer transition-experimental results. In: 9th AIAA/ASME Joint Thermophysics and Heat Transfer Conference, San Francisco, 5-8 June 2006. https://doi.org/10.2514/6.2006-2919
14. Ozalp C, Pinarbasi A, Sahin B (2010) Experimental measurement of flow past cavities of different shapes. Exp Therm Fluid Sci 34(5):505–515. https://doi.org/10.1016/j.expthermflusci.2009.11.003
15. Sudarshan B, Deep S, Jayaram V et al (2019) Experimental study of forward-facing cavity with energy deposition in hypersonic flow conditions. Phys Fluids 31(10):106105. https://doi.org/10.1063/1.5118751
16. Guvernyuk S, Simonenko M, Zubkov A (2021) Experimental study of supersonic flow around an axisymmetric annular cavity at angles of attack. Acta Astronaut 180:693–700. https://doi.org/10.1016/j.actaastro.2021.01.013
17. Sharipov F, Seleznev V (1998) Data on internal rarefied gas flows. J Phys Chem Ref Data 27(3):657–706. https://doi.org/10.1063/1.556019
18. Bird GA (1994) Molecular gas dynamics and the direct simulation of gas flows. Oxford University Press, Oxford
19. Schaaf SA, Chambré PL (1961) Flow of rarefied gases. Princeton University Press, Princeton
20. Palharini RC, Scanlon TJ, Reese JM (2014) Aerothermodynamic comparison of two-and three-dimensional rarefied hypersonic cavity flows. J Spacecr Rockets 51(5):1619–1630. https://doi.org/10.2514/1.A32746
21. Palharini RC, Scanlon TJ, White C (2018) Chemically reacting hypersonic flows over 3D cavities: Flowfield structure characterisation. Comput Fluids 165:173–187. https://doi.org/10.1016/j.compfluid.2018.01.029
22. Palharini RC, Santos WFN (2019) The impact of the length-to-depth ratio on aerodynamic surface quantities of a rarefied hypersonic cavity flow. Aerosp Sci Technol 88:110–125. https://doi.org/10.1016/j.ast.2019.03.007
23. Guo G, Luo Q (2018) DSMC investigation on flow characteristics of rarefied hypersonic flow over a cavity with different geometric shapes. Int J Mech Sci 148:496–509. https://doi.org/10.1016/j.ijmecsci.2018.09.022
24. Guo G, Chen H, Zhu L et al (2021) Investigation of hypersonic flows through a cavity with sweepback angle in near space using the DSMC method. Chin Phys B 30(7):074701. https://doi.org/10.1088/1674-1056/abf7ad
25. Guo G, Luo Q (2022) Numerical study of three-dimensional flow and aerodynamic characteristics of a cylindrical cavity in rarefied hypersonic flows. Int J Mech Sci 234:107703. https://doi.org/10.1016/j.ijmecsci.2022.107703
26. Guo G, Jiang S, Chen H et al (2022) Influence of flow control on aerodynamic properties of an open cavity in rarefied hypersonic flows. Acta Astronaut 191:404–416. https://doi.org/10.1016/j.actaastro.2021.11.036
27. Xiang S, Fang S (2022) DSMC study for effects of angles of attack on closed cavity of space vehicle in hypersonic rarefied flow. In: Ding H (eds) Aerospace mechatronics and control technology. Springer aerospace technology. Springer, Singapore. https://doi.org/10.1007/978-981-16-6640-7_4
28. Lekzian E (2023) Study of a non-reacting hypersonic flow over an external cavity with flow injection using DSMC method. Aerosp Sci Technol 140:108492. https://doi.org/10.1016/j.ast.2023.108492
29. Jiang Q, Cai G, Chen Y et al (2023) Effects of cavity shapes and sizes on rarefied hypersonic flows. Int J Mech Sci 245:108088. https://doi.org/10.1016/j.ijmecsci.2022.108088

30. Jin X, Huang F, Cheng X et al (2017) Numerical simulation for the effects of angles of attack on two- and three-dimensional rarefied hypersonic cavity flows using the direct simulation Monte Carlo method. In: 21st AIAA International Space Planes and Hypersonics Technologies Conference, Xiamen, 6-9 March 2017. https://doi.org/10.2514/6.2017-2401
31. Jin X, Wang B, Cheng X et al (2020) The effects of Maxwellian accommodation coefficient and free-stream Knudsen number on rarefied hypersonic cavity flows. Aerosp Sci Technol 97:105577. https://doi.org/10.1016/j.ast.2019.105577
32. Jin X, Wang B, Cheng X et al (2021) Effects of corner rounding on aerothermodynamic properties in rarefied hypersonic flows over an open cavity. Aerosp Sci Technol 110:106498. https://doi.org/10.1016/j.ast.2021.106498
33. Jin X, Huang F, Miao W et al (2021) Effects of the boundary-layer thickness at the cavity entrance on rarefied hypersonic flows over a rectangular cavity. Phys Fluids 33(3):036116. https://doi.org/10.1063/5.0045056
34. Jin X, Cheng X, Wang Q et al (2022) Numerical simulation for rarefied hypersonic flows over non-rectangular deep cavities. Phys Fluids 34(8):086108. https://doi.org/10.1063/5.0102685
35. Sazhin OV, Borisov SF, Sharipov F (2001) Accommodation coefficient of tangential momentum on atomically clean and contaminated surfaces. J Vac Sci Technol A 19(5):2499–2503. https://doi.org/10.1116/1.1388622
36. Sazhin OV, Borisov SF, Sharipov F (2002) Erratum:"Accommodation coefficient of tangential momentum on atomically clean and contaminated surfaces". J Vac Sci Technol A 20(3):957. https://doi.org/10.1116/1.1459081
37. Agrawal A, Prabhu SV (2008) Survey on measurement of tangential momentum accommodation coefficient. J Vac Sci Technol A 26(4):634–645. https://doi.org/10.1116/1.2943641
38. Cooper SM, Cruden BA, Meyyappan M et al (2004) Gas transport characteristics through a carbon nanotubule. Nano Lett 4(2):377–381. https://doi.org/10.1021/NL0350682
39. Keerthi A, Geim AK, Janardanan A et al (2018) Ballistic molecular transport through two-dimensional channels. Nature 558(7710):420–424. https://doi.org/10.1038/s41586-018-0203-2
40. Hsieh SS, Tsai HH, Lin CY et al (2004) Gas flow in a long microchannel. Int J Heat Mass Transfer 47(17-18):3877–3887. https://doi.org/10.1016/j.ijheatmasstransfer.2004.03.027
41. Sazhin O (2020) Rarefied gas flow into vacuum through a channel with sudden contraction or expansion. Microfluid Nanofluid 24(10):76. https://doi.org/10.1007/s10404-020-02384-w
42. Sazhin O (2020) Rarefied gas flow through a rough channel into a vacuum. Microfluid Nanofluid 24(4):27. https://doi.org/10.1007/s10404-020-2330-y
43. Sazhin O (2021) Gas outflow into vacuum over a forward-and backward-facing step in a wide range of rarefaction. Int J Heat Mass Transfer 179:121666. https://doi.org/10.1016/j.ijheatmasstransfer.2021.121666
44. Sazhin O, Sazhin A (2023) Rarefied gas flow into vacuum through linearly diverging and converging channels. Int J Heat Mass Transfer 203:123842. https://doi.org/10.1016/j.ijheatmasstransfer.2022.123842
45. Sazhin O, Sazhin A (2024) Transonic, supersonic, and hypersonic flow of rarefied gas into vacuum through channels with a forward- or backward-facing step. Microfluid Nanofluid 28(5):32. https://doi.org/10.1007/s10404-024-02727-x
46. Ivanov MS, Rogasinsky SV (1988) Analysis of numerical techniques of the direct simulation Monte Carlo method in the rarefied gas dynamics. Russ J Numer Anal Math Model 3(6):453–466. https://doi.org/10.1515/rnam.1988.3.6.453
47. Sazhin O (2008) Gas flow through a slit into a vacuum in a wide range of rarefaction. J Exp Theor Phys 107(1):162–169. https://doi.org/10.1134/S1063776108070170
48. Naris S, Valougeorgis D (2005) The driven cavity flow over the whole range of the Knudsen number. Phys Fluids 17(9):097106. https://doi.org/10.1063/1.2047549
49. Rossiter JE (1962) The effect of cavities on the buffeting of aircraft. RAE Technical Memorandum No Aero 754, Royal Aircraft Establishment, Farnborough
50. Stallings RL Jr, Wilcox FJ Jr (1987) Experimental cavity pressure distributions at supersonic speeds. NASA Technical Paper 2683, National Aeronautics and Space Administration, Hampton
51. Plentovich EB, Stallings RL Jr, Tracy MB (1993) Experimental cavity pressure measurements at subsonic and transonic speeds: Static-pressure results. NASA Technical Paper 3358, National Aeronautics and Space Administration, Hampton

Publisher's Note